CHEMISTRY OF MATERIALS

Article

pubs.acs.org/cm

Graphene Coatings for the Mitigation of Electron Stimulated Desorption and Fullerene Cap Formation

Alicja Bachmatiuk,[†,‡,§] Arezoo Dianat,[∥,⊥,#] Frank Ortmann,[∥,⊥,#] Huy Ta Quang,[†,▲] Magdalena Ola Cichocka,[†,▲] Ignacio Gonzalez-Martinez,[§,⊥] Lei Fu,[⬢] Bernd Rellinghaus,[⊥] Joergen Eckert,[§,⊥,▼] Gianaurelio Cuniberti,[∥,⊥,#,▼] and Mark Hermann Rümmeli*[,†,▲]

[†]IBS Center for Integrated Nanostructure Physics, Institute for Basic Science (IBS), Daejon 305-701, Republic of Korea

[‡]Centre of Polymer and Carbon Materials, Polish Academy of Sciences, M. Curie-Sklodowskiej 34, Zabrze 41-819, Poland

IFW Dresden, [§]Institute for Complex Materials and [⊥]Institute for Metallic Materials, P.O. Box 270116, D-01171 Dresden, Germany

[∥]Max Bergman Center of Biomaterials, [⊥]Institute of Materials Science, [#]Dresden Center for Computational Materials Science, and [▼]Center for Advancing Electronics Dresden, TU Dresden, 01062 Dresden, Germany

[▲]Department of Energy Science, Department of Physics, Sungkyunkwan University, Suwon 440-746, Republic of Korea

[⬢]College of Chemistry and Molecular Science, Wuhan University, 430072 Wuhan, China

Supporting Information

ABSTRACT: Graphene already has numerous applications in transmission electron microscopy. Here, we extend its application in electron microscopy by demonstrating its potential to stop electron induced desorption in nonconducting samples, where in essence charge build-up leads to surface atom desorption. Graphene films provide a conduction pathway to prevent charge build-up and do not interfere with the imaging process allowing the direct imaging of specimens sensitive to electron induced desorption. We also show that small graphene flakes on the surface of MgO transform to fullerenes or hemispherical fullerenes. The hemispherical fullerenes anchor to the MgO surface and are of particular interest as they suggest it should be possible to nucleate single walled carbon nanotubes on the surface of oxide supports without the need of a catalyst particle.

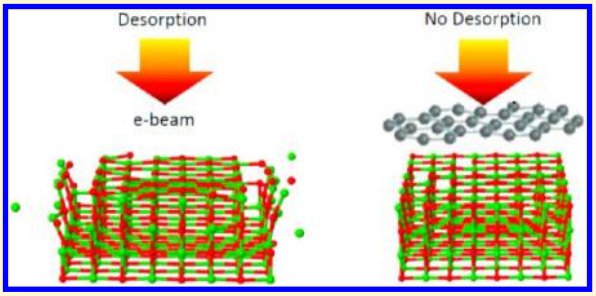

The isolation of graphene by Novoselov and Geim[1] in 2004 triggered mass interest in this material because of its amazing properties. It is believed that this material will eventually lead to remarkable applications in areas, such as biological engineering, optical electronics, ultrafiltration, composite materials, energy storage, and electronic devices. However, despite its great promise, real applications to date are somewhat limited, mostly because of technical difficulties, which, for the most part, one can anticipate will eventually be overcome.

A key area where graphene applications are already making an impact and continue to develop is its use as an aid material in transmission electron microscopy (TEM). For example, the implementation of graphene membranes as a microscope slide to suspend atoms and molecules for their observation provides significant advantages over traditional amorphous carbon membranes.[2−5] In addition, graphene membranes are excellent as cell windows for liquid cells,[6] for in situ investigations of graphene at high bias[7,8] and even as a template for the in situ catalyst-free growth of graphene and potentially of other 2D materials.[9] In this work, we extend the application of graphene as an aid for TEM by demonstrating its potential to significantly reduce the effects of electron induced desorption, thus reducing specimen damage from exposure to an electron beam in a TEM. In practice, the technique will also be useful to prevent specimen damage because of electron stimulated desorption in low energy electron diffraction (LEED) and reflection high energy diffraction (RHEED).

Several types of electron radiation damage can occur and they are discussed in greater detail by Egerton et al.[10] These interactions can be elastic or inelastic events. Elastic scattering events in which the incoming electrons are electro-statically deflected by the Coulomb field from each atomic nucleus can lead to atom displacement or sputtering (atom removal). Elastic scattering processes are also responsible for electron-diffraction patterns, and, diffraction and phase contrast in the observed images. Inelastic interactions also occur and take place through incoming electrons having Coulomb interactions with the atomic electrons that surround each nucleus. These interactions are better known for their analytical potential for electron energy loss spectroscopy (EELS) and the emission of

Received: June 4, 2014
Revised: August 10, 2014
Published: August 12, 2014

X-rays (e.g., energy dispersive X-ray spectroscopy (EDS)). They are also responsible for radiolysis effects which can change the structure of a sample or even remove material. However, here we focus on another radiation damage mechanism, mainly electron stimulated desorption. In this mechanism, low-energy secondary electrons (0−50 eV) and Auger electrons can be generated (10−200 eV) in the surface layers of a nonconducting specimen. This process leads to charging of the specimen, such that as the charge builds up, eventually, to compensate for the excess charge, positive ions are expelled from the surface of the material to re-establish electrostatic equilibrium.[11,12]

This process is, of course, a destructive process that can be undesirable if the goal is to investigate the specimen. One can overcome this process by coating the specimen with a conductive layer to enable electrostatic equilibrium to be reached without the need for ejecting surface material. However, this would normally interfere with the imaging of the specimen. To do this one needs a very thin material to minimize any interference with the specimen image and in addition the coating material should ideally be crystalline as this allows one to easily filter out the coating material (if needed) using fast Fourier transform filtering techniques. Graphene, which is only one atom thick is then the ultimate thin coating and is crystalline with a honeycomb lattice of C atoms. In addition, graphene is a zero-gap semiconductor and so conducts electrons very well. Thus, it would seem graphene is an ideal coating material for specimens sensitive to electron stimulated desorption.

To test this concept we choose MgO nanocrystals as our test sample because MgO does not suffer from knock on damage below 300 kV (the Mg knock-on damage threshold is 460 keV and for O 330 keV).[13−15] Moreover MgO has been shown to be sensitive to electron stimulated desorption through low-energy irradiation through the Knotek−Fiebelman (KF) mechanism.[16,17]

In the KF mechanism, charge builds up rapidly through multiple atomic Auger decay steps. With respect to MgO it is believed a valence electron of O^{2-}-ion Auger decays to a Mg^{2+}-2p core-hole to form a Mg^{+}-ion and O^{+}-ion with an energy release of 47 eV. This process is illustrated in Figure 1. Thus, the now positive surface aided by further electron-atom interactions can eject an O^{+}-ion, followed by an exposed Mg^{+}-ion both of which were produced by the KF mechanism.[16] MgO is also a choice material for this initial study as we have already shown one can easily coat MgO nanocrystals by CVD at low temperatures, and thus not damage the nanocrystals.[18,19] During these studies we also examined MgO nanocrystals that were only partially covered with graphene. As expected with only graphene patches on the surface electron induced desorption is not reduced since there is no clear conduction path. However, very small graphene flakes were found to transform instantaneously in to fullerenes or hemispherical caps at the MgO surface. The transformation of very small graphene flakes to fullerenes has been demonstrated previously over graphene.[20] However, the formation of hemispherical Fullerene caps at crystal surfaces has not been reported and holds interest in understanding the nucleation of single walled carbon nanotubes over oxides.

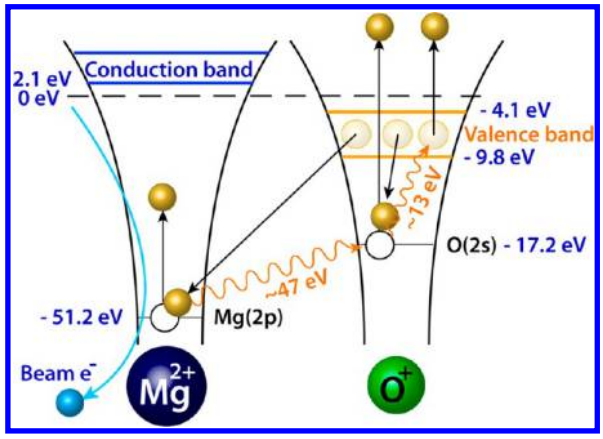

Figure 1. Schematic illustrating the KF multiple atomic Auger decay routes in MgO upon electron irradiation. From left to right: Initially an electron is ejected from Mg; this ejected electron can then induce electron ejection from oxygen species.

We begin by showing the efficiency with which electron induced desorption can remove material from MgO. This can be seen in movie 1 provided in the Supporting Information and in Figure 2. In Figure 2, various TEM micrographs show the erosion of MgO nanocrystals after 5, 40, and 50 s. In addition the erosion rates appear to differ depending on the surface termination as can be seen by comparing the upper and lower arrows in the first and last panels of Figure 2 (left side). The upper arrow indicates the (100) face while the lower one points to the (111) face. Indeed, the (100) face erodes faster than the (111) face in a layer by layer manner (movie 1, Supporting Information, shows the process in far more detail).

To better comprehend the process we conducted molecular dynamics simulations of the electron induced desorption process. We first look at the electron induced desorption dependence on the electron beam dose. The results for this are presented in Figure S1 in the Supporting Information. They show increased desorption with increasing electron beam dose. This is in agreement with experimental work by Zhang et al.[16] which shows a linear dependence of decomposition with dose. We then investigate the role of crystal orientation and electron induced desorption. We do this implementing charge injection (dose) of 0.4 electrons per atom into the nanocrystals of MgO with (100) and (111) orientations. First principle molecular dynamics (FPMD) were used to describe the time evolution of the charged systems. Because of strong repulsive electrostatic forces, the nanocrystals decompose through the successive desorption of individual atoms from the surfaces, affecting equally both O and Mg species. No clear correlation between desorption events of individual atoms are observed, however the erosion is most effective at the edges of both crystal orientations. On the other hand, the FPMD simulations do show a clear difference between the (100) face and the (111) as can be seen in Supporting Information movies 2 and 3, respectively, and in Figure 2 (right side). In agreement with our experimental findings we find erosion of atoms from the surface occurs faster on the (111) face than the (100) face. This is because of the layer like structure that occurs for the (111) orientation, in which oxygen and magnesium alternate. Given the strong ionic character of the bonding, this gives rise to alternating negatively and positively charged layers along the [111] direction. Such charged layers are relatively unstable surface terminations, which accelerates the erosion process. Indeed, our simulations show an enhanced average desorption rate by 41% from a (111) surface (24 atoms/ps) compared to the (100) orientation (17 atoms/ps).

dx.doi.org/10.1021/cm502043x | *Chem. Mater.* 2014, 26, 4998−5003

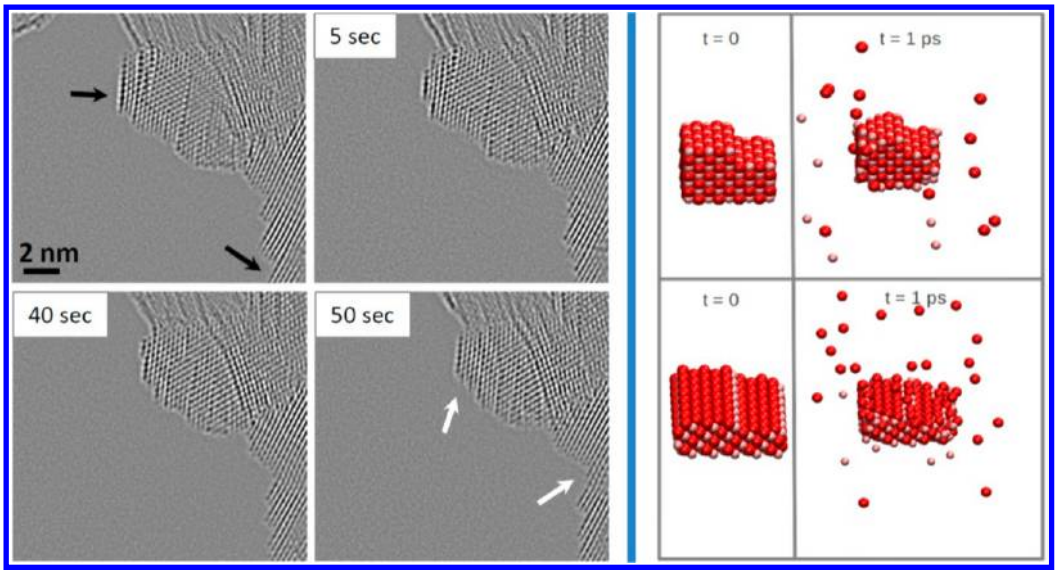

Figure 2. Left panels: Selected micrographs from movie 1 (Supporting Information) showing electron induced desorption of MgO nanocrystals after 5, 40, and 50 s. The top and bottom arrows highlight (100) and (111) faces, respectively. Right panels: Molecular dynamics simulations showing electron induced desorption for the (100) orientation (top) and (111) orientation (bottom).

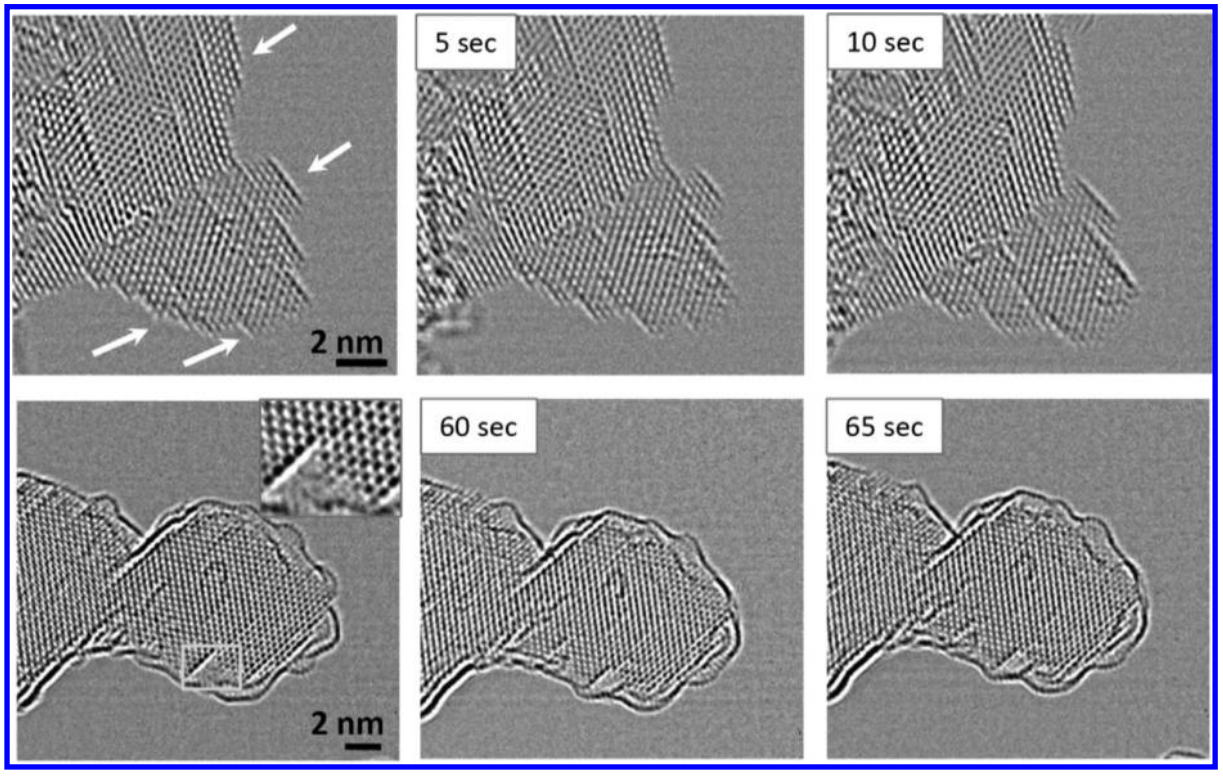

Figure 3. Top row: Micrographs showing significant electron induced desorption of MgO after only 5 and 10 s. Bottom row: Micrographs showing the stability of MgO coated in graphene even after 60 and 65 s.

We now turn to the case of MgO nanoparticles encapsulated with graphene. The lower panels of Figure 3 show an MgO nanocrystal encapsulated in graphene after irradiation for 60 and 65 s almost no damage can be discerned whereas as without a graphene coating even after only 5 and 10 s (see top panels of Figure 3) damage can be easily observed. This clearly demonstrates the advantage of coating specimens sensitive to electron induced desorption with graphene to significantly reduce the desorption process since the graphene provides an efficient conduction path to prevent charge build up. Moreover, the MgO crystal structure is not compromised by the graphene coating as can be seen by the level of detail in the inset of the bottom left panel. Indeed, the graphene sheet is nearly indistinguishable from the vacuum in agreement with findings from ref 21 so that direct imaging of the specimen is possible because graphene has equipotential conductive surface which minimizes any phase distortion to the traversing (imaging) electron wave. Even if the graphene lattice did contribute to the image its contribution could easily be subtracted using fast Fourier transform masking techniques.[3,21] Another aspect of

dx.doi.org/10.1021/cm502043x | *Chem. Mater.* 2014, 26, 4998−5003

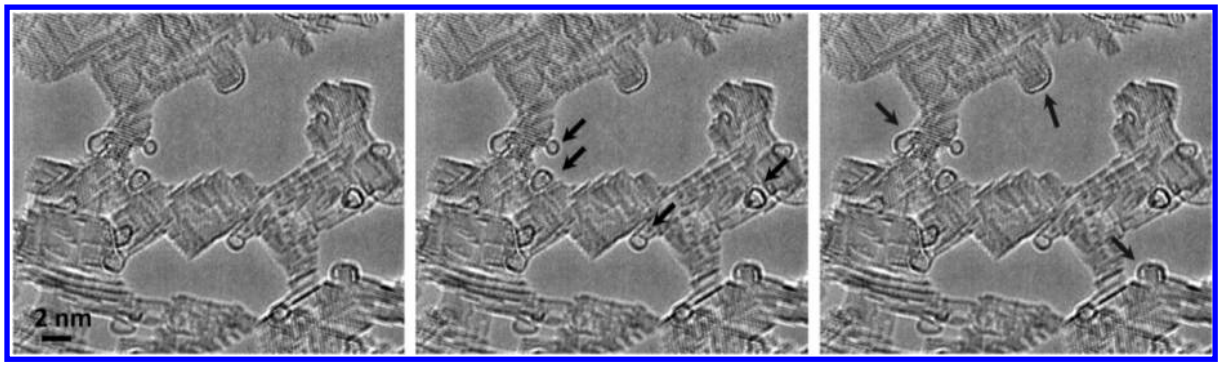

Figure 4. Micrograph showing an assortment of fullerenes and hemispherical fullerenes (caps) on the surface of MgO nanocrystals. Fullerenes are highlighted in the middle panel and caps are highlighted in the right panel.

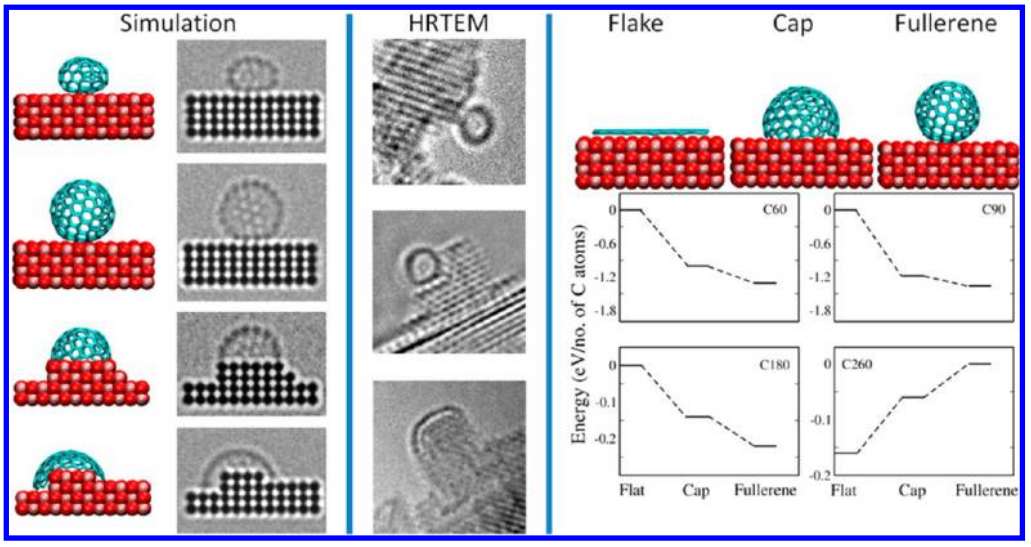

Figure 5. Left: Stick and ball models and corresponding image simulations of fullerenes and caps on MgO surfaces. Middle: HRTEM images of fullerenes and a cap. Right: Ab initio results for the total energy for graphene flake versus cap and fullerene formations over MgO for 60, 90, 180, and 260 carbon atoms, respectively.

these samples is that they are fully coated with graphene and so the curved edges and graphene lying in-plane with the beam leads to a dark contrast at the edges of the coated specimen. However, as can be seen in the lower panels of Figure 3, these edges for the most part do not significantly prevent any loss of edge information from the specimen due to the van der Waals gap between the specimen and the graphene coatings. Moreover, graphene coatings do not necessarily need to be formed by CVD as we demonstrate here. In principle graphene coatings in which layers of graphene cover the specimen through polymer-based transfer techniques would have less edge contrast forming or if the specimen were loaded on to a TEM grid with a graphene membrane in which no edge contrast would be expected.

In some of our samples where only short CVD reaction times were applied to the MgO nanocrytals, the nanocrystals do not get fully coated with graphene but instead form little graphene nanoislands on the surface as we have shown previously.[18] In addition, sometimes structures resembling fullerenes and fullerene hemispherical caps with their ends attached to the MgO surface can be observed. Figure 4 shows some representative examples as well as figure S2 in the Supporting Information. Detailed studies of the as-produced material using Raman spectroscopy do not show any signature that would indicate the presence of fullerenes[18] and more over we are not aware of any reports of fullerene production by CVD.

In short, the presence of fullerenes by CVD synthesis is unexpected. To be sure these structures are concomitant with fullerenes and hemispherical fullerenes, we prepared image simulations of such structures, and as can be seen form a few examples in Figure 5 (left side), they match very well with the experimental observations (middle), namely, fullerenes and hemispherical caps are present. Thus, the question is how do these structures arise? Recently, it was shown that graphene flakes that are sufficiently small and reside on graphene, can transform directly into fullerenes under electron irradiation (80 kV electron acceleration voltage). This occurs through the loss of carbon atoms at the edge, followed by the formation of pentagons which triggers the formation of a hemispherical structure which subsequently zips up its open edges to form a fullerene.[20] Thus, it is entirely feasible that a similar process occurs for small graphene flakes residing on MgO. In addition, the same process could explain the formation of the hemispherical fullerene structures we observe at MgO surfaces. The main difference being in this case, that here unsaturated bonds at the surface of MgO exist, while in the case of the study on graphene, such surface states are not available to trap a fullerene cap before closure in to a complete fullerene.

dx.doi.org/10.1021/cm502043x | *Chem. Mater.* 2014, 26, 4998−5003

To better comprehend the process and its feasibility we conducted ab initio total energy calculations to determine the relative formation energies for fullerenes and hemispherical fullerenes at different MgO surface morphologies. In the first study we investigated the formation energy of a fullerene against a fullerene cap formation over a MgO ridge, at a ridge and at a flat MgO surface, and as shown in Figure S3 (Supporting Information) the lowest energy occurs for a fullerene formation and the highest for a cap formation at a smooth (100) surface with an energy difference of ∼0.6 eV. Moreover, the energy difference between fullerene and hemispherical caps at ridged surfaces is only ∼0.3 eV indicating both are likely. This is in agreement with our experimental observations where caps are usually found at ridges along with fullerenes.

Within the ab initio studies we also investigated the effect of the size of the initial graphene flake on the surface of MgO. In this study the formation energies for different initial graphene flake sizes was investigated (60, 90, 180, and 260 atoms). The transformation energies for both cap and fullerene formation were studied. The results are summarized in Figure 5. The data shows that for 60 and 90 atoms the energy difference between a fullerene or cap formation and a flat graphene flake is ∼1.5 eV and either a cap or fullerene is favored. This remains true for 180 atoms, however the energy difference is smaller (∼0.2 eV) and by the time one reaches 260 atoms, it becomes preferable for the graphene flake to remain flat. This is in keeping with studies of graphene flakes on graphene, which also suggest large flakes to not transform because the energy penalty to induce curvature is too high.[20] Moreover, this is in excellent agreement with our experimental observations.

In summary, we show proof of principle that the use of graphene coatings as a means to prevent destruction of samples sensitive to electron induced desorption. In essence the graphene provides a conduction pathway to prevent charge build up that would ultimately lead to surface atom displacement. In addition the graphene coating does not interfere with imaging the specimen, thus, allowing direct observation of the specimen to be conducted. The implementation of graphene coatings will also be useful to prevent electron stimulated desorption in sensitive samples for LEED and RHEED diffractometry where desorption during measurement can distort the data. In this study we coat the MgO nanoparticles with low temperature CVD. Alternative coating processes could be through the well-established process of depositing graphene using polymer based transfer on to a specimen or my transferring the specimen directly on to a TEM grid with a graphene membrane.

We also show that very small nanoflakes on the surface of MgO can transform to fullerenes or hemispherical fullerenes (carbon caps). These carbon caps anchor the MgO surface. Such carbon caps are a prerequisite for carbon nanotube nucleation and suggest that carbon nanotubes could be grown directly on oxide supports without the need for catalyst particles.

EXPERIMENTAL SECTION

The MgO nanocrstals were purchased from Alfa Aesar (purity = 99.99%). The graphene coating and deposition of graphene flakes was accomplished using a purpose-built CVD reactor. For the CVD reaction a nominal amount of MgO powder was placed inside a crucible with was then loaded into the horizontal quartz tube in a furnace. Initially the reactor was evacuated down to 1 hPa and the oven heated to the desired reaction temperature. Then, the carbon feedstock (acetylene) mixed with argon was introduced (100 kPa, 600 sccm). Reaction temperatures of between 325 and 875 °C were used. Reaction times varied between 30 and 300 s. The TEM investigations were conducted in a third-order aberration corrected (objective lens) FEI Titan 300−80 operating with an acceleration voltage of 80 kV. Low-pass filtering has been applied to the micrographs to reduce noise. The filtering does not affect the final resolution of the images because of significant oversampling of the original images. The multislice TEM image simulations were performed using JEMS software. For the simulations an acceleration voltage of 80 kV and an energy spread of 0.3 eV was used.

Density functional theory approaches were used for the total energy calculations as well as molecular dynamics (MD) simulations by means of a mixed Gaussian and plane wave method using the cp2k code.[22] The PBE plane wave functional and the DZVP (double-ζ for valence electrons plus polarization function) localized basis sets were used. The energy cutoff was set to 300 Ry for the plane wave expansion of the density. For the total energy calculations, the two top layers of MgO surfaces as well as carbon based structures are allowed to relax and bottom layers are kept fixed. The geometry optimization for the carbon nanostrucures on surfaces are performed using periodic boundary conditions with a vacuum gap of about 15 Å in the slab direction. MD simulations are performed for the MgO clusters with (100) and (111) surface orientations with an induced charge of 0.4 e^-/atoms.

ASSOCIATED CONTENT

Supporting Information

Supporting data from molecular dynamics (MD) simulations, additional experimental TEM data, and MD and TEM movies. This material is available free of charge via the Internet at http://pubs.acs.org.

AUTHOR INFORMATION

Corresponding Author

*E-mail address: mark@rummeli.com.

Author Contributions

A.B. and A.D. contributed equally.

Notes

The authors declare no competing financial interest.

ACKNOWLEDGMENTS

The research was supported by the Institute of Basic Sciences, Korea and the Sino-German Center for Research Promotion (Grants GZ 871), as well as the excellence cluster CFAED (Dresden). All are gratefully acknowledged. A.B. thanks the Foundation for Polish Science for the financial support within the frames of the Homing Plus Programme (Grant agreement HOMING PLUS/2013-7/2).

REFERENCES

(1) Novoselov, K. S. *Science* **2004**, *306*, 666−669.
(2) Lee, Z.; Jeon, K. J.; Dato, A.; Erni, R. T.; Richardson, J.; Frenklach, M.; Radmilovic, V. *Nano Lett.* **2009**, *9*, 3365−3339.
(3) Meyer, J. C.; Girit, C. O.; Crommie, M. F.; Zettl, A. *Nature* **2008**, *454*, 319−322.
(4) Schaeffel, F.; Wilson, M.; Bachmatiuk, A.; Ruemmeli, M. H.; Queitsch, U.; Rellinghaus, B.; Briggs, G. A. D.; Warner, J. W. *ACS Nano* **2011**, *5*, 1975−1983.
(5) Nair, R. R.; Blake, P.; Blake, J. R.; Zan, R.; Anissimova, S.; Bangert, U.; Golovanov, A. P.; Morozov, S. V.; Geim, A. K.; Novoselov, K. S.; Latychevskaia, T. *Appl. Phys. Lett.* **2010**, *97*, 153102.
(6) Jong, M. Y.; Park, J. W.; Ercius, P.; Kim, K. P.; Hellebusch, D. J.; Crommie, M. F.; Lee, J. Y.; Zettl, A.; Alivisatos, A. P. *Science* **2012**, *336*, 61−64.

(7) Boerrnert, F.; Barreiro, A.; Wolf, D. M.; Katsnelson, I.; Buechner, B.; Vandersypen, M. K. L.; Rummeli, M. H. *Nano Lett.* **2012**, *12*, 4455−4459.
(8) Barreiro, A.; Boerrnert, F.; Rummeli, M. H.; Buechner, B.; Vandersypen, L. M. K. *Nano Lett.* **2012**, *12*, 1873−1878.
(9) Boerrnert, F.; Avdoshenko, S. M.; Bachmatiuk, A.; Ibrahim, I.; Buechner, B.; Cuniberti, G.; Rummeli, M. H. *Adv. Mater.* **2012**, *24*, 5630−5635.
(10) Egerton, R. F.; Li, P.; Malac, M. *Micron* **2004**, *35*, 399−409.
(11) Gonzalez-Martinez, I.; Gorantla, S. M.; Bachmatiuk, A.; Bezugly, V.; Zhao, J.; Gemming, T.; Kunstmann, J.; Eckert, J.; Cuniberti, G.; Rümmeli, M. H. *Nano Lett.* **2014**, *14*, 799−805.
(12) Cazaux, J. *Ultramicroscopy* **1995**, *60*, 411−425.
(13) Youngman, R. A.; Hobbs, L. W.; Mitchell, T. E. *J. Phys. (Paris)* **1980**, *41*, C6−227−331.
(14) Hobbs, L. W. *Ultramicroscopy* **1979**, *3*, 381−386.
(15) Dupuy, C. H. S. *Radiation Damage Processes in Materials*, 88th ed.; Chemical Rubber Co., Boca Raton, FL, 2008; p. 309.
(16) Zhang, H. R.; Egerton, R.; Malac, M. *Nucl. Instr. Meth. B* **2013**, *316*, 137−143.
(17) Kramer, J.; Ernst, W.; Tegenkamp, C. H. *Pfnnür Surf. Sci.* **2002**, *517*, 87−97.
(18) Rummeli, M. H.; Bachmatiuk, A.; Scott, A.; Boerrnert, F.; Warner, J. H.; Hoffman, V.; Lin, J. H.; Cuniberti, G.; Buechner, B. *ACS Nano* **2010**, *4*, 4206−4210.
(19) Scott, A.; Dianat, A.; Boerrnert, F.; Bachmatiuk, A.; Zhang, S.; Warner, J. H.; Borowiak-Palen, E.; Knupfer, M.; Buechner, B.; Cuniberti, G.; Rummeli, M. H. *Appl. Phys. Lett.* **2011**, *98*, 73110/1−3.
(20) Chuvilin, A. *Nat. Chem.* **2010**, *2*, 450−453.
(21) Lee, Z. *Nano Lett.* **2009**, *9*, 3365−3369.
(22) CP2K Open Source Molecular Dynamics, 2014. http://www.cp2k.org/.